

AEOL-Induced NRF2 Activation and DWORF Overexpression Mitigate Myocardial I/R Injury

Antonio Lax

alax@um.es

University of Murcia <https://orcid.org/0000-0001-5452-8781>

Maria del Carmen Asensio Lopez

Biocardio SL

Miriam Ruiz Ballester

University of Murcia

Silvia Pascual Oliver

Biomedical Research Institute Virgen de la Arrixaca (IMIB-Arrixaca)

Maria Josefa Fernandez del Palacio

Department of Animal Medicine and Surgery. University of Murcia

Yassine Sassi

Fralin Biomedical Research Institute.

Jose Javier Fuster

Centro Nacional de Investigaciones Cardiovasculares (CNIC)

Domingo Pascual Figal

Heart Failure Unit, Cardiology Department, University Hospital Virgen de la Arrixaca

Fernando Soler

University of Murcia

Article

Keywords: acute myocardial infarction, reperfusion injury, NRF2, SERCA2a, PLN, DWORF, AEOL-10150, cardiac protection

Posted Date: May 15th, 2024

DOI: <https://doi.org/10.21203/rs.3.rs-4358850/v1>

License:   This work is licensed under a Creative Commons Attribution 4.0 International License. [Read Full License](#)

Additional Declarations: (Not answered)

Abstract

The causal relationship between the activation of NRF2 and the preservation of SERCA2a function in mitigating myocardial ischemia-reperfusion (I/R) injury, along with the associated regulatory mechanisms, remains incompletely understood. The aim of this study was to characterize this relationship by testing the pharmacological repositioning of AEOL-10150 (AEOL) as a novel NRF2 activator. C57BL6/J, *Nrf2* knockout (*Nrf2*^{-/-}), and wild-type (*Nrf2*^{+/+}) mice, as well as human induced pluripotent stem cell-derived cardiomyocytes (hiPSCMs) were subjected to I/R injury. Gain/loss of function techniques, RT-qPCR, western blotting, LC/MS/MS, and fluorescence spectroscopy were utilized. Cardiac dimensions and function were assessed by echocardiography. In the early stages of I/R injury, AEOL administration reduced mitochondrial ROS production, decreased myocardial infarct size, and improved cardiac function. These effects were due to NRF2 activation, leading to the overexpression of the micro-peptide DWORF, consequently enhancing SERCA2a activity. The cardioprotective effect induced by AEOL was diminished in *Nrf2*^{-/-} mice and in *Nrf2/Dworf* knockdown models in hiPSCMs subjected to simulated I/R injury. Our data show that AEOL-induced NRF2-mediated upregulation of DWORF disrupts the phospholamban-SERCA2a interaction, leading to enhanced SERCA2a activation and improved cardiac function. Taken together, our study reveals that AEOL-induced NRF2-mediated overexpression of DWORF enhances myocardial function through the activation of the SERCA2a offering promising therapeutic avenues for I/R injury.

Introduction

Acute myocardial infarction (AMI), triggered by thrombotic occlusion of a coronary artery, is a leading cause of morbidity and disability worldwide¹. Current treatment strategies for AMI rely on percutaneous coronary intervention (PCI) to rapidly restore coronary artery blood flow. Unfortunately, this reperfusion procedure can itself trigger profound myocardial injury, additional to that caused by the preceding ischemia, and the compound effects of this myocardial ischemia–reperfusion (I/R) injury include cardiomyocyte death, cardiac dysfunction, and ventricular remodeling^{2–5}. An analysis of AMA data from 2008 showed that, despite timely PCI, approximately 10% of AMI patients died during their index hospitalization and 25% of survivors developed chronic heart failure (CHF)⁶. Current treatments for CHF, including vasodilators, loop diuretics, and inotropic agents, help to alleviate congestion and improve hemodynamics in the short-term. However, there is a lack of drugs able to prevent end-organ damage or improve long-term outcomes in AMI patients treated by PCI⁷. It is therefore vital to explore novel therapeutic options to alleviate ventricular remodeling and prevent progression to CHF.

Extensive research over four decades has shown that I/R-injury is mediated by two major mechanisms, oxidative damage and cytosolic Ca²⁺ overload^{8–10}. A crucial role in these processes is played by nuclear factor erythroid 2-related factor 2 (NRF2), a key transcription factor in the cellular antioxidant response¹¹. NRF2 regulates the expression of a series of genes involved in defense against oxidative damage, including antioxidant enzymes and detoxifying proteins¹². NRF2 activation can counteract mitochondrial oxidative damage¹³ and preserve the function of essential proteins such as sarcoplasmic reticulum (SR) Ca²⁺-ATPase (SERCA2a)¹⁴. SERCA2a, whose activity is regulated by the accessory protein phospholamban

(PLN) and the micropeptide DWORF¹⁵⁻¹⁷, plays a key role in cardiac muscle by pumping Ca²⁺ from the cytosol to the SR, directly influencing heart contraction and relaxation¹⁸. PLN acts as a natural SERCA2a inhibitor, whereas DWORF activates SERCA2a by binding to it and displacing PLN¹⁷. Disturbance of SERCA2a function, particularly under conditions of oxidative stress¹⁹, leads to Ca²⁺ accumulation in the cytosol, resulting in contractile dysfunction and intracellular Ca²⁺ dysregulation²⁰. Although there is substantial evidence for a functional connection between NRF2 and SERCA2a, the mechanism of this relationship remains incompletely understood. There is thus a need to characterize how NRF2 directly or indirectly influences SERCA2a function, as well as the roles played by PLN and DWORF in this setting. Furthermore, NRF2 activation holds promise as an innovative approach to cardiac protection¹².

The metalloporphyrin AEOL-10150 (AEOL), a mimic of the catalytic site of superoxide dismutase, provides protection against radiation-induced lung injury²¹ and enhances myocardial function in mice undergoing anthracycline-based chemotherapy²². The protective role of AEOL appears to involve multiple mechanisms of action, including antioxidant²³, anti-inflammatory²⁴, and anti-fibrotic activities, indicating a potential therapeutic benefit in MI/R injury. In the present study, we assessed the impact of AEOL on NRF2 and its role as a modulator of SERCA2a activity via PLN and DWORF during MI/R injury.

Methods

Preparation of human iPS-derived cardiomyocytes (hiPSCMs) and simulated I/R model. Human induced pluripotent stem cells (hiPSCs) were purchased from Phenocell (PCi-CAU); $\sim 0.5 \times 10^5$ viable cells were provided in cryovials. hiPSCs were initially grown to 80% confluence in mTeSR™ plus medium on Matrigel® matrix to allow attachment of cell aggregates and maintained in a humidified 95% air, 5% CO₂ atmosphere at 37°C. When the cells reached passage 20, the reprogramming procedure was started using our standardized protocol. Briefly, the culture medium was removed and replaced with RPMI-1640 containing B27 supplement minus insulin (basal differentiation supplement) and 4 μM CHIR99021 (day 0). On day 3, the medium was changed to basal differentiation supplement containing 3 μM of IWR-1. On day 5, the medium was refreshed with basal differentiation supplement. The medium was replaced on day 8 with fresh RPMI 1640 containing B27 supplement minus insulin. On day 11, the medium was changed to glucose-free RPMI 1640 containing B27 supplement minus insulin. On day 14, the medium was reverted to RPMI 1640 containing B27 supplement minus insulin. Differentiation cultures were maintained in a 95% air, 5% CO₂ atmosphere at 37°C. During differentiation, the medium was replaced every 3 days. Beating clusters were observed after 20 days. hiPSCMs were allowed to recover for 12 days in iCell Maintenance Medium (Cellular Dynamics International) before experiments. Before assays, standardized RT-qPCR gene expression profiles were determined for hiPSCs and derived hiPSCMs (Figure S1). OCT4 and NANOG were used as hiPSC-specific markers and cTnT and NKX 2–5 as hiPSCM-specific markers.

The I/R model was adapted with modifications from the experimental design of Sebastião et al.²⁵. In brief, ischemia was mimicked by replacing iCell medium with ischemia-mimetic solution (140 mM NaCl, 12 mM KCl, 1.2 mM MgCl₂, 20 mM HEPES, 1.8 mM CaCl₂, 20 mM sodium lactate, pH 6.22) and placing the hiPSCMs cultures in a hypoxia chamber (STEMCELL Technologies; 27310) at 37°C in a nitrogen-enriched atmosphere

to achieve a 1% O₂ concentration. After 45 min of simulated ischemia, reperfusion was mimicked by reoxygenation in control culture conditions (iCell medium at 21% O₂), which were maintained for a recovery period of 24 h. Control cultures were maintained throughout experiments in iCell medium at 21% O₂. When indicated, 50 μM AEOL or 30 nM DWORF were added at the onset of reoxygenation. At the end of the 24 h reoxygenation–recovery period, cells were processed for subsequent analysis. For succinate treatment, hiPSCMs were incubated in assay buffer (132 mM NaCl, 10 mM HEPES, 4.2 mM KCl, 1 mM MgCl₂, 1.8 mM CaCl₂, 2.5 μM 2-deoxyglucose, 1.14 sodium pyruvate, pH 7.4) and treated with the indicated agents in the presence or absence of 5 mM dimethyl succinate or 4 μM oligomycin for 2 h.

Animal care and ethics. Male C57Bl/6J mice (25–30 g) were purchased from the ENVIGO Laboratory. Colonies of Nfe2l2tm1Ywk (*Nrf2*) knockout mice (*Nrf2*-KO) and *Nrf2*-WT littermates were from the Jackson Laboratory. *Nrf2* gene knockout was confirmed by genotyping with the Jackson Laboratory-recommended protocol and primers: *Nrf2* common_forward (5′-GCCTGAGAGCTGTAGGCC-3′), *Nrf2* WT_reverse (5′-GGAATGGAAAATAGCTCCTGCC-3′), and *Nrf2* Mut_reverse (5′-GACAGTATCGGCCTCAGGAA-3′). Animals were housed in a specific pathogen-free environment at 23 ± 2°C and 50 ± 5% relative humidity and with a 12 h light–dark cycle. Mice had free access to food and water. All animal experiments were approved by the Ethics Review committee for animal use at the University of Murcia (approval No. A13220701). Animals were adapted to the environment for 7 days before experimentation.

In vivo myocardial I/R model and experimental design. Mice were anesthetized and ventilated via tracheal intubation with a Harvard rodent respirator. The left anterior descending coronary artery was ligated with a 6–0 silk suture slip knot positioned approximately 2 mm below the edge of the left atrial appendage. MI/R injury was initiated by tightening the slip knot to induce ischemia, followed after 45 min by release of the knot to produce myocardial reperfusion and recovery for 30 min, 24 h, 28 days (4 weeks), or 56 days (8 weeks). The animals were randomly assigned to receive AEOL (25 mg/kg in physiological saline solution (0.9% NaCl)) or vehicle (saline solution only), administered via subcutaneous injection after reperfusion onset. The AEOL dose was based on a published analysis of *in vivo* efficacy in mice²⁶. The study comprised two distinct phases. The initial phase aimed to examine the protective effects of AEOL against acute-phase MI/R injury (Figure S2, Experiment 1). Mice subjected to MI/R received a single dose of AEOL or vehicle at 15 min after reperfusion onset and were then allowed to recover for either 30 min or 24 h (Figure S2; Experiment 1). The second part of the study explored the long-term benefits of AEOL on adverse cardiac remodeling. A separate cohort of mice underwent MI/R and received daily repeat injections of AEOL or vehicle for 5 days, starting at 5 min, 15 min, or 3 days after reperfusion onset (Figure S2; Experiment 2). These mice were allowed to recover for either 4 or 8 weeks. When indicated, mice received intraperitoneal injections of 30 nM DWORF coincident with AEOL treatment.

Measurement of mitochondrial ROS in vitro and in vivo. To measure mitochondrial ROS production in hiPSCMs, 3x10⁶ cells suspended in DPBS were incubated for 20 min at 25°C with the fluorescent probe MitoSox (Invitrogen) at 5 μM. The cells were then washed and centrifuged (480 xg, 10 min), and changes in fluorescence intensity were measured at λ_{ex} = 510 nm and λ_{em} = 580 nm in a Clariostar microplate reader (BMG Labtech). Mitochondrial ROS production was plotted as the relative increase in fluorescence.

Mitochondrial ROS production in the hearts of mice subjected to ml/R injury was estimated from the conversion of the ratiometric probe MitoB to MitoP²⁷. Briefly, 25 nmol MitoB (Cayman Chemical; 17116) in 100 μ L DPBS was administered via tail vein injection 4 h before initiating the ml/R protocol (with or without AEOL injection 15 min after reperfusion onset). After reperfusion and recovery for 30 min or 24 h, hearts were removed. The infarct border zone was processed and flash frozen in liquid nitrogen. Heart tissue samples were homogenized, spiked with deuterated internal standards [d_{15} -MitoB (Cayman Chemical; 17470) and d_{15} -MitoP (Cayman Chemical; 19296)], and MitoB and its product MitoP were determined by liquid chromatography and tandem mass spectrometry. The MitoP/MitoB ratio was plotted as the relative increase relative to sham operated mice.

Measurement of oxidative DNA damage. DNA samples were prepared from the infarct border zone 30 min after ml/R, incubated at 95°C for 5 min, and rapidly chilled on ice to prevent re-annealing of single-stranded DNA. The DNA was then digested with 5 units of nuclease P1 in 20 mM sodium acetate, pH 5.2 for 2 h at 37°C. Next, samples were resuspended in 100 mM Tris buffer, pH 7.5 and treated with 5 units of alkaline phosphatase for 1 h at 37°C. The reaction mixtures were centrifuged for 5 min at 6,000 \times g, and the supernatants were analyzed by competitive ELISA for 8-hydroxy-2'-deoxy guanosine (8-OHdG) (OxiSelect™ Oxidative DNA Damage ELISA Kit; Cell Biolabs STA-320-T). Absorbance was read at 450 nm in a Clariostar microplate reader (BMG Labtech), and the fold change in 8-OHdG was plotted relative to sham-operated mice.

Mitochondrial function and cell viability. hiPSCMs were subjected to simulated I/R with or without AEOL treatment at the onset of reoxygenation. At the end of the 24-h reoxygenation period, the conditioned medium was collected for lactate assay (Abcam; ab653331), and the cells were harvested for the determination of ATP content with the ATP Luminometric Assay kit (Beyotime Institute of Biotechnology). Total protein was determined by the bicinchoninic acid (BCA) method²⁸. To measure mitochondrial membrane potential ($\Delta\psi_m$), hiPSCMs were loaded with TMRE (500 nm) (Abcam; ab113852) for 30 min at 37°C. Cells were then washed twice with warm DPBS containing 0.2% bovine serum albumin (BSA) (w/v), and fluorescence intensity was detected in a plate reader with excitation/emission at 549/575 nm. MPTP opening was assayed with the Mitochondrial Transition Pore Assay Kit (Life Technology). Cell viability was measured with the Cell Counting Kit-8 (Enzo; ALX-850-039). Measurements and analysis were carried out in a Clariostar microplate reader (BMG Labtech).

TUNEL assay of ml/R-induced apoptotic cell death. In mice at 24 h post-ml/R, hearts were arrested in diastole by intravenous injection of a 0.2 mL bolus of 30% (w/v) KCl (Merck). The hearts were excised and rinsed with ice-cold DPBS before removal of the right ventricle and atria. Mid-papillary slices of the left ventricle (n = 7 mice per treatment group) were fixed in 4% (w/v) formaldehyde for up to 24 h before paraffin embedding. The slices were stained by terminal deoxynucleotidyl transferase dUTP nick end labeling (DeadEnd colorimetric TUNEL system, Promega Corporation). Apoptotic cells were identified by dark-brown precipitation in cardiomyocyte nuclei, visualized in high-power visual fields (400X) with an Axioscope Axio A10 brightfield microscope (Carl Zeiss) fitted with a high-resolution color digital camera (AxioCam 506 color). Representative images were obtained with Zeiss Zen, version 3.0 (Cals Zeiss).

Assessment of myocardial infarct size. Mice at 8 weeks post-mI/R were given a KCl bolus as above to arrest the heart in diastole. After sacrifice, hearts were excised, rinsed in ice-cold DPBS, and frozen by immersion in liquid nitrogen for 10 min. Frozen mid-papillary slices (1–3 mm) of the LV of seven mice from each treatment group were immersed in 1% 2,3,5-triphenyl-tetrazolium chloride (TTC; Merck) in DPBS at 37°C for 15 min to stain the non-infarcted tissue. The slices were photographed, and the perimeters of the left ventricle and the infarcted area were traced manually on digital images and measured with ImageJ software (National Institutes of Health). The size of the infarcted area was calculated as the percentage of the left ventricle and expressed as the fold difference from control.

Echocardiography analysis of heart function. Mice were examined before surgery (baseline) and at 1, 4, and 8 weeks post-mI/R by transthoracic echocardiography under anesthesia (1-1.5% isoflurane) by a blinded trained investigator (MJFP). Images were acquired with a Vevo 3100 high-frequency ultrasound imaging system (VISUALSONICS, Inc, Toronto, Canada) fitted with a 30-MHz central frequency transducer and connected to an integrated rail system III. All echocardiographic parameters were measured according to recommendations of the ESC Working Group on Myocardial Function in Adult Rodents²⁹. LV end-diastolic and end-systolic dimensions were measured by parasternal short-axis M-mode echocardiography, and FS was calculated using the ultrasound machine program; LV internal diameters at end diastole (LVIDd) and end systole (LVIDs) and EF were calculated in 2D mode from the right parasternal four-chamber long-axis view, using the modified Simpson method. Pulsed Doppler parameters of mitral inflow (early peak diastolic velocity (E), late peak diastolic velocity (A), and the E/A ratio) were measured in apical four-chamber view. Pulsed Doppler tissue parameters measured at the mitral septal annulus were peak systolic velocity (S'), early peak diastolic velocity (E'), and late peak diastolic velocity (A'), and the E/E' ratio was calculated. Isovolumic relaxation time (IVRT) was measured from synchronous left ventricular outflow tract flow and mitral flow and used to calculate the E/IVRT ratio.

Protein sample preparation. Fresh LV tissue (~ 30 mg) from the infarct border zone of mice 24 h after mI/R or hiPSCMs (~ 8×10^6 cells) were washed in cold DPBS and processed for the isolation of subcellular protein fractions (see Supplementary Material) or gently homogenized in RIPA buffer (Thermo Fisher) supplemented with 100-fold diluted protease and phosphatase inhibitors to obtain the total protein fraction. Homogenates were centrifuged at 20,000 xg at 4°C for 20 min, protein concentration in the supernatants was measured by the BCA method²⁸, and samples were aliquoted and stored at -80°C.

Western blotting. Proteins (35 µg) were denatured, separated by SDS-PAGE, and transferred to a polyvinylidene difluoride (PVDF) membrane (Merck Millipore, USA). Non-specific sites were blocked by incubating membranes with 5% (w/v) BSA in TBST (137 mM NaCl, 20 mM Tris, and 0.1% (v/v) Tween-20, pH 7.6), followed by overnight incubation at 4°C with primary antibodies in blocking buffer. Membranes were then washed 5 times for 10 min each with TBST and incubated for 1 h at room temperature (RT) with the appropriate secondary antibody in blocking buffer. After a further 5 more 10 min washes in TBST, immunoreactive bands were detected by enhanced chemiluminescence (Amersham ECLTM Primer Western Blotting Detection Reagent

(GE Healthcare) (RPN2232), using a ChemiDoc XRS + system with Image Lab software from Bio-Rad Laboratories. Band density was quantified with Gel-Pro Analyzer 3.1 software (Sigma). Molecular weight was determined by comparison with prestained protein markers (Precision Plus Protein™ Dual Color Standards, Bio-Rad 1610374). Equal loading was monitored with antibodies to GAPDH (for cytosolic fractions) or H3 (nuclear fractions). Antibodies and their dilutions, sources, and references are summarized in Table 1.

Table 1
Antibodies and dilutions.

	Protein	Provider	Code	Dilution
Antibodies	1° Bax	Cell Signaling	#2772	1:4000
	Bcl2	Cell Signaling	#3498	1:2000
	NRF2 (D1Z9C)	Cell Signaling	#12721	1:1000
	Phospho- PLN	Badrilla	A010-12AP	1:3000
	PLN	Badrilla	A010-14	1:10000
	DWORF	Mybiosource	MBS5400388	1:5000
	SERCA 2a	Cell Signaling	#4388	1:1000
	GAPDH	SIGMA	G9545-100UL	1:5000
	Keap1	Cell Signaling	#8047	1:5000 (cells)
	P62	Cell Signaling	#5114	1:5000
	LC3A/B	Cell Signaling	#4108	1:2000
	HO-1	Cell Signaling	#43966	1:2000
	Histone H3	Cell Signaling	#9715	1:1000
	2° ECL Mouse IgG, HRP-linked whole Ab	Promega	W402B	1:10000
ECL Rabbit IgG, HRP-linked whole Ab	Promega	W401B	1:5000	

In vitro knockdown. hiPSCMs were transfected with specific siRNAs targeting *NRF2* (Accell Human NFE2L2 siRNA, DHARMACON) or *DWORF* (SIRGT66230WQ-2OMe, CREATIVE BIOLABS) using Lipofectamine™

MessengerMAX™ Transfection reagent (Thermo Fisher). Cells were seeded 2 days before transfection in 6-well plates with 2 mL STEMdiff Cardiomyocyte Support Medium (STEMCELL Technologies) at 60% confluence. Stock transfection mixes were prepared according to the manufacturer's instructions. In brief, 9 µL Lipofectamine reagent was diluted in 141 µL Opti-MEM I Medium (Invitrogen) and incubated for 5 min at RT. In another tube, siRNAs or a scrambled control RNA oligonucleotide were diluted with Opti-MEM to a final concentration of 25 nM. The mixes were then combined and incubated for 30 min at RT to allow the formation of RNA–lipid complexes. For transfections, the STEMdiff Cardiomyocyte Support Medium was removed and replaced with 1.75 mL fresh medium and 250 µL of the appropriate transfection mix. The cells were incubated at 37°C for 48 h, after which they were washed twice with DPBS at 37°C before ischemia. Transfection efficiency was determined and is shown in Figure S3.

RNA extraction and quantitative RT-PCR. Fresh samples of LV infarct border zone (~ 30 mg) from mice at the indicated time after MI/R or hiPSCMs (2 x10⁶ cells) were washed with cold DPBS. Cells were pelleted by centrifugation at 480 ×g for 10 min at 4°C, whereas tissue samples were placed in a pre-chilled glass Petri dish in an ice bath and chopped with sharp scissors. RNA was extracted with the RNeasy Mini Kit (QIAGEN), and cDNA was prepared with the iScript cDNA Synthesis Kit (Bio-Rad). Quantitative real time polymerase chain reaction (RT-qPCR) was performed with the TB Green Premix Ex Taq II (Tli RNase H Plus) Master Mix (Takara Bio). Glyceraldehyde 3-phosphate dehydrogenase (*GAPDH*) was used as the housekeeping control gene. Primers were obtained from Merck, and sequences are listed in Table 2.

Table 2
Primer sequences used for quantitative real-time PCR analysis

	Primer	Forward (5'-3')	Reverse (5'-3')
Human	<i>GAPDH</i>	TCAACGACCACTTTGTCAAGCTCA	GCTGGTGGTCCAGGGGTCTTACT
	<i>NANOG</i>	CATGAGTGTGGATCCAGCTTG	CCTGAATAAGCAGATCCATGG
	<i>NKX 2-5</i>	CTACGGTTATAACGCCTACCC	CGAAGTTCACGAAGTTGTTGTT
	<i>NRF2</i>	GCGCAGACATTCCCGTTTGT	GCTCTCGATGTGACCGGGAA
	<i>OCT4</i>	TCTTTCCACCAGGCCCCCGGCTC	TGCGGGCGGACATGGGGAGATCC
	<i>cTnT</i>	GGCAGCGGAAGAGGATGCTGAA	GAGGCACCAAGTTGGGCATGAACGA
	<i>DWORF</i>	TTCTTCTCCTGGTTGGATGG	TCTTCTAAATGGTGTGAGATTGAAGT
Mouse	<i>Nrf2</i>	TGCTCGGACTAGCCATTGCC	GTCTTGCCTCCAAAGGATGTCA

Co-immunoprecipitation. hiPSCM extracts (8 × 10⁶ cells/extract) were collected and incubated overnight with an antibody to PLN (Badrilla, A010-14, 1:100), SERCA (Cell Signaling, 4388, 1:100) or DWORF (Mybiosource, MBS5400388, 1:500) at 4°C with gentle shaking. To the incubation was added 20 µL of protein A–Sepharose slurry, followed by further incubation for 4 h at 4°C with gentle shaking. The beads were then washed 3 times with immunoprecipitation (IP) buffer (20 mM HEPES pH 7.4, 0.5 mM EDTA, 150 mM NaCl, and 0.1% Triton X-100) to remove non-specifically bound proteins. In each wash, the beads were

mixed gently with IP buffer and centrifuged for 10 min at 480 xg and 4°C, and the supernatant was discarded. To elute antigen–antibody complexes, the beads were resuspended in 25 µL SDS gel-loading buffer and heated at 95°C for 4 min. After this, samples were separated by SDS-PAGE at 30 mA constant current for 2 h. Immunocomplexes were analyzed by western blotting with primary antibodies to SERCA2a (Cell Signaling, 4388, 1:1000), PLN (Badrilla, A010-14, 1:10000), or DWORF (Mybiosource, MBS5400388, 1:5000). IgG was used as a control.

Isolation of microsomal fractions and determination of SERCA2a activity. Microsomal fractions enriched in sarcoplasmic reticulum (SR) vesicles were isolated as described in ³⁰, with modifications. LV tissue samples (~80 mg wet weight) obtained from the infarct border zone of mice 24 h after MI/R were homogenized in liquid nitrogen using a pestle and mortar in 10 mM NaCO₃ at 1:20 dilution, supplemented with protease inhibitors and phosphatase inhibitors. The homogenate was incubated on ice for 20 min and centrifuged at 5,900 xg for 10 min at 4°C, and the supernatant was collected and centrifuged at 51,000 xg for 60 min at 4°C. The resulting supernatant (cytosolic fraction) was discarded, and the pellet was resuspended in 0.6 mM KCl and resedimented at 100,000 xg for 40 min to obtain the microsomal fraction (SR vesicles). Protein concentration was measured by the BCA method ²⁸, and samples were aliquoted and stored at – 80 °C until use.

SERCA2a activity was assayed in 96-well microplates using an enzyme-coupled, NADH-linked ATPase assay ³¹ with modifications. Each well contained assay mix (50 mM MOPS pH 7.0, 100 mM KCl, 5 mM MgCl₂, 1 mM EGTA, 0.2 mM NADH, 1 mM phosphoenol pyruvate, 10 IU/mL pyruvate kinase, 10 IU/mL lactate dehydrogenase, 1 µM A23187, 1 mM CaCl₂ (free Ca²⁺, 10 µM), and 0.02 mg SR protein/mL). The assay was started by adding ATP to a final concentration of 5 mM (200 µL total assay volume/well), and absorbance was measured at 340 nm in a Clariostar microplate reader (BMG Labtech). As a control, SERCA pump activity was blocked with 100 nM thapsigargin ³². Samples were tested in triplicate.

Measurement of circulating sST2. Plasma samples isolated from mice 24 h after MI/R were assayed for sST2 levels, as previously described ³³ using an ELISA kit (Quantikine ELISA Mouse ST2/IL33R (MST200); R&D Systems, USA). Measurement at 24 h post-MI/R was based on a previous study showing an increase in circulating sST2 in acute-phase injury ³³. Reactions were terminated by addition of a stop solution, and absorbance was determined at 450 nm in a Clariostar microplate reader (BMG Labtech). Intra- and inter-assay precision in term of coefficient of variation were less than 10%.

Statistical analysis. Data are reported as mean ± SEM. Statistical differences were evaluated by fitting linear models, with interactions determined by one-way ANOVA followed by post hoc testing with the Bonferroni correction. Differences were considered significant at p < 0.05.

Results

AEOL reduces reperfusion-induced succinate-driven mitochondrial ROS production

We postulated that pharmacological scavenging of mitochondrial ROS (mtROS) by AEOL-10150 (hereafter AEOL) during ml/R would limit reperfusion-related injury, reduce cardiac remodeling, and protect against CHF. In the cellular model of simulated I/R, ischemia followed by reoxygenation triggered a significant increase in mtROS production by human iPS-derived cardiomyocytes (hiPSCMs) that was blocked by treatment with AEOL at the onset of reoxygenation ($p < 0.001$) (Fig. 1A). Since mtROS generation during reperfusion is driven by succinate³⁴; in separate experiments we treated hiPSCMs with cell-permeable dimethyl succinate and the ATP synthase inhibitor oligomycin, to mimic reperfusion-mediated mtROS production. In the context of the high $\Delta\Psi_m$ induced by ATP synthase inhibition, succinate fueled extensive mtROS generation, which was reduced by AEOL (Fig. 1B). To investigate the effect of AEOL on cardiac mtROS production during ml/R *in vivo*, we used a model of left anterior descending coronary artery ligation and reperfusion (Figure S2; experimental groups – 1a and – 1b) in mice previously injected with the mitochondria-targeted ROS probe MitoB.

Treatment with AEOL 15 min after reperfusion onset prevented mtROS production during the early injury phase (30 min; Fig. 1D), resulting in attenuation of oxidative DNA damage (Figure S4A). Similar results were obtained when mtROS levels were measured at 24 h post-reperfusion (Figure S4B).

Short-term post-reperfusion AEOL therapy attenuates acute I/R injury and prevents adverse cardiac remodeling

Mitochondrial function was impaired in the hiPSCM I/R model, as indicated by MPTP opening and collapse of the $\Delta\Psi_m$ (Fig. 2A-B). This resulted in activation of the mitochondrial apoptotic pathway, evidenced by upregulation of Bax protein expression and downregulation of Bcl2 (Figure S5A). These alterations were prevented by AEOL treatment during the reoxygenation/recovery phase, which also attenuated cell death (Fig. 2C), reduced lactate accumulation, and restored hiPSCM ATP content (Figure S5B-C).

AEOL also decreased myocardial apoptosis in infarcted mice (Fig. 2D). Administration of AEOL either 5 min (Fig. 2E and 2F) or 15 min after reperfusion onset (Fig. 2E and 2G) and maintained through daily injections for the first 6 days after ml/R was able to reduce infarct size at 8 weeks. However, no cardioprotective effect was observed when AEOL administration was initiated later, starting at 3 days post-ml/R (Fig. 2E and 2H). When AEOL therapy was initiated in the acute-phase (15 min post-ml/R), mice developed significantly less cardiac hypertrophy at 8 weeks than mice treated with vehicle ($p < 0.01$) (Fig. 3A-B). Taken together, these data suggest that short-term AEOL therapy after ml/R is protective and produces beneficial long-term outcomes.

Table 3
Echocardiographic parameters for cardiac functions

		EXPERIMENTAL GROUPS					
		Sham (n = 10)	C57BL6/ml/R+ vehicle (n = 14)	C57BL6/ml/R+ AEOL (n = 14)	<i>Nrf2</i> KO/ ml/R+ Vehicle (n = 8)	<i>Nrf2</i> KO/ ml/R+ AEOL (n = 10)	<i>Nrf2</i> - KO/ ml/R+ AEOL+ DWORF (n = 7)
		Post-ml/R (1 weeks)					
VARIABLES	HR (bpm)	423.80 ± 10.46	415.90 ± 11.82	440.50 ± 9.38	419 ± 10.28	402.43 ± 9.94	441.29 ± 21.26
	LVEdD (mm)	3.97 ± 0.04	4.51 ± 0.02*	4.16 ± 0.01&	4.61 ± 0.13	4.52 ± 0.01	4.14 ± 0.00#
	LVEsD (mm)	2.50 ± 0.07	3.33 ± 0.04*	2.65 ± 0.02&	3.55 ± 0.12	3.24 ± 0.01	2.63 ± 0.01#
	FS (%)	40.49 ± 0.38	27.53 ± 0.54*	36.42 ± 0.10&	25.95 ± 0.99	28.24 ± 0.06	36.36 ± 0.05#
	FE (%)	75.66 ± 0.88	60.12 ± 0.16*	72.36 ± 0.08&	59.41 ± 0.53	60.66 ± 0.12	71.72 ± 0.34#
	CO (ml/min)	15.37 ± 0.36	10.62 ± 0.29*	12.54 ± 0.17&	10.15 ± 0.39	10.41 ± 0.23	12.78 ± 0.27#
	S (mm/s)	20.76 ± 0.93	17.68 ± 0.67*	20.26 ± 1.07&	16.65 ± 1.03	17.61 ± 0.76	22.06 ± 1.21#
	E/A	1.47 ± 0.03	1.96 ± 0.09*	1.46 ± 0.04&	1.95 ± 0.09	1.97 ± 0.10	1.52 ± 0.05#
	E/E'	30.98 ± 1.76	41.13 ± 1.16*	33.64 ± 2.87&	39.95 ± 1.60	40.95 ± 1.10	33.09 ± 1.17#
	E/IVRT	37.26 ± 0.97	20.35 ± 0.73*	36.53 ± 1.07&	22.56 ± 1.69	20.77 ± 0.82	38.55 ± 0.95#
		Post-ml/R (4 weeks)					
	HR (bpm)	412.00 ± 11.37	395.65 ± 43.83	455.10 ± 2.44	446.29 ± 9.60	432.86 ± 11.81	444.00 ± 9.32
	LVEdD (mm)	3.94 ± 0.08	4.83 ± 0.02*	4.34 ± 0.03&	4.89 ± 0.05	4.79 ± 0.01	4.37 ± 0.03#
	LVEsD (mm)	2.38 ± 0.03	3.66 ± 0.02*	2.88 ± 0.02&	3.68 ± 0.06	4.08 ± 0.43	2.90 ± 0.02#
	FS (%)	40.20 ± 0.35	23.84 ± 0.04*	33.34 ± 0.06&	23.59 ± 0.23	23.95 ± 0.02	33.49 ± 0.05#

FE (%)	75.08 ± 0.86	54.10 ± 0.27*	68.43 ± 0.11&	52.72 ± 2.02	60.66 ± 0.45	63.85 ± 4.44#
CO (ml/min)	15.38 ± 0.52	10.28 ± 0.64*	12.81 ± 0.32&	10.63 ± 0.67	11.87 ± 0.89	13.30 ± 0.51#
S (mm/s)	20.54 ± 1.11	17.31 ± 0.62*	22.71 ± 0.60&	18.28 ± 0.43	17.16 ± 0.79	22.72 ± 0.69#
E/A	1.39 ± 0.04	2.03 ± 0.13*	1.63 ± 0.09&	1.95 ± 0.13	2.01 ± 0.14	1.81 ± 0.09#
E/E´	28.50 ± 1.41	43.84 ± 1.22*	32.26 ± 1.69&	38.04 ± 2.04	47.08 ± 5.84	37.54 ± 1.19#
E/IVRT	39.98 ± 2.63	22.40 ± 1.08*	36.28 ± 1.11&	22.45 ± 1.41	23.90 ± 2.78	33.01 ± 1.133
Post-mi/R (8 weeks)						
HR (bpm)	427.50 ± 7.45	453.00 ± 18.30	423.70 ± 12.11	439 ± 6.84	440.29 ± 9.75	445.43 ± 7.74
LVEdD (mm)	3.96 ± 0.04	4.98 ± 0.01*	4.37 ± 0.04&	5.02 ± 0.10	4.92 ± 0.01	4.38 ± 0.01#
LVEsD (mm)	2.38 ± 0.04	3.74 ± 0.05*	2.98 ± 0.01&	3.59 ± 0.07	3.75 ± 0.02	2.98 ± 0.02#
FS (%)	39.92 ± 0.24	23.33 ± 0.13*	31.70 ± 0.19&	24.01 ± 0.37	23.52 ± 0.05	32.12 ± 0.07#
FE (%)	76.58 ± 0.38	52.88 ± 0.14*	66.57 ± 0.08&	54.42 ± 1.16	52.93 ± 0.21	66.43 ± 0.15#
CO (ml/min)	13.91 ± 0.33	9.61 ± 0.21*	12.74 ± 0.43&	9.88 ± 0.09	9.53 ± 0.17	12.70 ± 0.41#
S (mm/s)	20.53 ± 0.93	17.42 ± 0.70*	21.73 ± 0.93&	16.85 ± 1.13	16.55 ± 0.52	23.99 ± 0.53#
E/A	1.42 ± 0.05	1.90 ± 0.09*	1.53 ± 0.06&	1.88 ± 0.04	1.80 ± 0.03	1.72 ± 0.03#
E/E´	29.38 ± 1.35	44.96 ± 2.76*	32.00 ± 3.31&	41.28 ± 4.57	36.73 ± 0.36	47.51 ± 2.21#
E/IVRT	38.12 ± 2.35	21.30 ± 0.79*	32.35 ± 1.96&	19.49 ± 0.57	18.55 ± 1.03	34.89 ± + 0.48#

To test whether these differences in post-mi/R cardiac enlargement correlate with changes in cardiac structure and function, we examined mice by echocardiography. Acute-phase treatment with AEOL, with 6 daily injections starting at 15 min after mi/R, significantly reduced the severity of adverse remodeling detected after 8 weeks ($p < 0.001$) (Fig. 3B, Table 3). Compared with vehicle-treated mice, AEOL-treated mice had smaller left ventricular (LV) internal diameters at end diastole (LVIDd) and end systole (LVIDs),

accompanied by better % ejection fraction (% EF) and % fractional shortening (% FS). These functional and structural data thus demonstrate that AEOL reduces infarct expansion, improves outcomes, and limits progression to HF when therapy was initiated in the acute-phase (15 min post-mI/R).

AEOL preserves the feed-forward loop linking NRF2, Keap1, and p62 after mI/R

To investigate the mechanism of the cardioprotective effect of early post-mI/R AEOL, we examined the effect on the p62–Keap1–NRF2 antioxidative signaling pathway. As early as 1-day post-mI/R, cytosolic and nuclear NRF2 localization in the myocardium was significantly decreased relative to sham-operated mice (Fig. 4A-B) ($p < 0.001$ in both cases). This change was paralleled by decreases in the protein expression of Keap1 and p62 (Fig. 4C-D) ($p < 0.001$) and an increase in the cardiac LC3 II/I ratio (Fig. 4E) ($p < 0.01$). Furthermore, the disruption of the p62–Keap1–Nrf2 feed-forward loop after mI/R resulted in direct impairment of antioxidant capacity, manifested as significantly reduced protein expression of HO-1 (Fig. 4F) ($p < 0.001$) and the increased mtROS production presented in Fig. 1. AEOL treatment significantly increased p62 expression and normalized the LC3 II/I ratio ($p < 0.001$ in both cases). Cardiac nuclear NRF2 expression was significantly higher in AEOL-treated mI/R mice than in the vehicle-treated mI/R group ($p < 0.001$), although the Keap1 expression was further decreased by AEOL therapy ($p < 0.01$).

Close analysis of NRF2 activity and expression after mI/R revealed a surge in NRF2 activity and mRNA expression 15 min after reperfusion onset, followed by a decline to 24 h post-reperfusion (Figure S6). Treatment with 6 daily injections of AEOL starting at 15 min after mI/R sustained a significantly higher NRF2 activity than observed in control animals ($p < 0.001$), and this activation was maintained throughout the 8-week study period (Figure S6A). These findings indicate that interventions targeting NRF2 activation after mI/R should be administered early after reperfusion.

AEOL-induced NRF2 activation protects against I/R-induced cardiac injury

Given the ability of AEOL to preserve the feed-forward loop linking NRF2, Keap1, and p62 during the acute injury phase, we next investigated the possible involvement of NRF2 in the cardioprotective effect of AEOL therapy. *Nrf2* knockout (KO) mice and (WT) littermate controls were treated or not with 6 daily injections of AEOL starting at 15 min after mI/R and assessed for mI/R injury after 8 weeks. Infarcts were larger in *Nrf2*-KO mice than in WT controls ($p < 0.001$), and whereas AEOL reduced infarct size in WT mice ($p < 0.001$), it had no effect in the *Nrf2*-KO mice. The same effect was evident when infarct size was expressed as a proportion of the area-at-the-risk (AAR, Fig. 5B-C). Moreover, infarcted *Nrf2*-KO mice had much higher plasma levels of myocardial overload marker sST2 at 24 h post-mI/R than their WT counterparts, indicating more severe cardiac injury, and plasma sST2 was not reduced by AEOL therapy in the *Nrf2*-KO mice (Fig. 5D).

Comparable results were obtained in the hiPSCM I/R model. Specific siRNA silencing of human *NRF2* prevented AEOL-induced protection against increases in c-TnT, LDH, and sST2 after ischemia–

reoxygenation ($p < 0.001$, in all cases) (Fig. 5E). These findings collectively suggest that AEOL exerts its cardioprotective action through modulation of NRF2.

NRF2 improves cardiac contractility and prevents adverse cardiac remodeling through upregulation of DWORF protein expression

In WT mice, ml/R reduced the protein expression of the SERCA2a activator DWORF measured in the infarct border zone 24 h after reperfusion onset ($p < 0.001$), and this effect was prevented by AEOL treatment at 15 min post-ml/R ($p < 0.001$). *Nrf2*-KO mice had lower baseline DWORF expression than WT mice, and this expression was unaffected by the ml/R procedure with or without post-reperfusion AEOL treatment ($p < 0.001$ in all cases) (Fig. 6A). Similar results were obtained in the simulated I/R model in hiPSCMs (Fig. 6B), with AEOL ameliorating the ischemia–reoxygenation-induced decrease in DWORF expression ($p < 0.001$). As in the mouse ml/R model, suppression of NRF2 expression reduced DWORF expression and blocked the effect of AEOL ($p < 0.001$).

We next tested the effect of NRF2-induced DWORF overexpression on the phosphorylation state of PLN, its interaction with SERCA2a, and cardiac contractility. Phosphorylation of PLN at Ser¹⁶ was decreased at 24 h post-ml/R in WT mice ($p < 0.001$), and this change was not prevented by AEOL treatment (Figure S7A). The same pattern was observed in *Nrf2*-KO mice ($p < 0.001$), indicating that PLN phosphorylation is insensitive to NRF2 and the presence of AEOL (Figure S7A). Comparable results were obtained in hiPSCMs, with simulated I/R injury decreasing PLN phosphorylation, AEOL treatment during reoxygenation unable to prevent it, and *Nrf2* knockdown having no effect (Figure S7B).

Co-immunoprecipitation analysis in hiPSCMs revealed that simulated I/R induced the formation of SERCA2a–PLN complexes, that AEOL treatment prevented the accumulation of these complexes, and that the effect of AEOL was annulled by silencing of endogenous NRF2 or DWORF protein expression ($p < 0.001$ in all cases) (Fig. 6C-D). Addition of exogenous DWORF protein to hiPSCMs with suppressed NRF2 expression restored the AEOL sensitivity of SERCA–PLN interaction ($p < 0.001$). In contrast, interaction between SERCA2a and DWORF was decreased after simulated I/R, and this decrease was prevented by AEOL treatment during reoxygenation ($p < 0.001$, in all cases) (Fig. 6E-F). The effect of AEOL was blocked by silencing of NRF2 or DWORF ($p < 0.001$), and addition of exogenous DWORF protein reverted the effect of siNRF2 ($p < 0.001$).

Having established the ability of AEOL to regulate SERCA2a–PLN interaction through the cardiac micropeptide DWORF, we next investigated whether the DWORF–PLN interplay was able to regulate SERCA2a activity in the chronic phase after ml/R injury. SERCA2a activity was reduced at 24 h post-ml/R in both WT and *Nrf2*-KO mice ($p < 0.001$), and this effect was prevented by AEOL treatment at 15 min post-ml/R in WT mice ($p < 0.001$) but not in *Nrf2*-KO mice (Fig. 7). Injection of DWORF in *Nrf2*-KO mice at the same time as AEOL overcame the blockade of AEOL-mediated protection of SERCA2a activity ($p < 0.001$) (Fig. 7) and improved cardiac function (Table 3).

Discussion

This study demonstrates the potential applicability and therapeutic efficacy of AEOL in mitigating ml/R injury and preventing CHF. Our results provide evidence that AEOL-mediated acute activation of NRF2 protects against ml/R injury and establish a causal link between AEOL-induced NRF2 activation and upregulated expression of the micropeptide DWORF, resulting in enhanced SERCA2a pump action and improved cardiac function. Our data also support the idea that DWORF serves as a direct activator of SERCA2a by displacing PLN from the SERCA2a complex at the onset of reperfusion.

For the present study, we sought to mimic the clinical scenario of myocardial remodeling, which is characterized by oxidative damage and a major pathophysiological impact of intracellular Ca^{2+} overload. The *in vivo* mouse model of 45 min occlusion of the left anterior descending coronary artery followed by reperfusion and recovery produced large infarct areas, occupying about 40% of the left ventricle and producing signs of CHF at 8 weeks post-reperfusion. Despite rapid interventional reperfusion strategies, a similar outcome can occur in patients with ST-segment elevation myocardial infarction, particularly those reperfused after prolonged ischemia or with low or no coronary reflow³⁵, conditions strongly associated with poor long-term outcomes.

Our research primarily focused on the role of NRF2 activation in mitigating ml/R injury, given its significance as a key defense mechanism against oxidative damage and mitochondrial dysfunction^{13,36}. Reductions in cardiac nuclear translocation of NRF2 and the expression of HO-1 and p62 were accompanied by upregulated autophagy, increased apoptosis, and cardiac dysfunction after ml/R injury, effects that were prevented by AEOL treatment early after reperfusion onset. ROS accumulation increases significantly during the acute phase of cardiac reperfusion, triggering a reparative response associated with NRF2 activation³⁷. Unfortunately, this activation is transient, as evidenced by our finding of a substantial decline in *Nrf2* mRNA levels and activity just 24 h post-reperfusion. Enhancing NRF2 activity, including approaches promoting NRF2 nuclear translocation, is thus an attractive cardioprotective strategy with potential application in AMI³⁷⁻³⁹. While previous studies examined AEOL's potential to mitigate radiation-induced lung injury in large animal models^{21,23,40,41}, alleviate anthracycline-induced cardiotoxicity²², and even reduce ischemic brain damage⁴², ours is the first study to explore the potential applicability and therapeutic efficacy of AEOL in mitigating cardiac ml/R injury and preventing CHF. Our results confirm that AEOL-induced cardioprotection during ml/R injury is largely dependent upon NRF2 activation and also define the most effective therapeutic intervention window, revealing that AEOL administered within 15 min of reperfusion onset, but not later, effectively attenuated mtROS production and averted oxidative DNA damage to cardiac tissue. Moreover, our findings provide compelling evidence that AEOL heightens mitochondrial performance and promotes cell viability, resulting in smaller infarcts and preserved myocardial function. These findings demonstrate the potential clinical utility of repurposing AEOL as a cardioprotective agent able to mitigate the deleterious effects of acute-phase reperfusion injury.

Our study also firmly establishes the mechanistic relationship between the protective effect of AEOL and NRF2-pathway activation. The ability of AEOL to limit infarct expansion, adverse LV remodeling, and HF progression was abolished by *Nrf2* gene knockout; moreover, AEOL-induced NRF2 activation upregulated

the expression of the micropeptide DWORF, a potent regulator of myocardial contractility via enhanced SERCA2a activity⁴³, achieved by displacing the SERCA-2a inhibitor PLN. Enhancement of SERCA-2a activity is concomitant with prominent Ca²⁺-loading of the sarcoplasmic reticulum and improved Ca²⁺ signal parameters, including an increase in the transient Ca²⁺ peak amplitude and a reduced cytosolic Ca²⁺ influx decay time in each contraction–relaxation cycle⁴⁴. Upregulated DWORF expression has been shown to restore Ca²⁺ cycling and cardiac function in a mouse model of dilated cardiomyopathy⁴⁴ and can promote cardioprotection in isolated rat hearts subjected to I/R⁴³; however, no previous study confirmed a cardioprotective effect of DWORF administered during cardiac reperfusion after an ischemic event *in vivo* or identified the factors controlling cardiac DWORF expression. Although our study did not focus on the detailed molecular mechanism, our data provide evidence of a causal relationship between NRF2 activation and cardiac DWORF upregulation after MI/R. Blocking NRF2 expression, through gene knockout in *Nrf2*-KO mice or siRNA gene silencing in hiPSCMs, abrogated AEOL-induced DWORF upregulation without affecting the phosphorylation status of PLN. This is an important observation given the blockade of SERCA2a activation in AEOL-treated *Nrf2*-KO mice after MI/R. This result can be explained by the ability of DWORF to activate SERCA2a by displacing PLN, regardless of its phosphorylation state¹⁷, as suggested by our data analysis. Treatment with DWORF in combination with AEOL in the acute reperfusion phase restored SERCA2a activation in *Nrf2*-KO mice and prevented subsequent development of systolic and diastolic dysfunction, mimicking the effect of AEOL treatment alone in wild-type mice.

Our study demonstrates the therapeutic potential of AEOL as a modulator of the NRF2–DWORF pathway, ultimately leading to preserved cardiac contractility, reduced myocardial injury, and protection against HF development. These results have direct clinical implications, demonstrating that AEOL, administered early during reperfusion, holds the potential to revolutionize the management of AMI patients by mitigating reperfusion-induced injury and improving long-term cardiac outcomes. Further research and clinical trials are warranted to validate and translate these promising preclinical findings into effective treatments for AMI patients.

Study limitations

While our study establishes a causal link between AEOL-induced NRF2 activation and DWORF upregulation, the mechanism through which NRF2 induces DWORF expression remains to be elucidated. Secondly, whereas NRF2 is known to be activated by heightened ROS levels, our analysis did not address the specific mechanism of AEOL-induced NRF2 activation. Further studies are warranted to explore this intriguing phenomenon.

Abbreviations

$\Delta\Psi_m$ Mitochondrial membrane potential

AMI Acute myocardial infarction

CHF Chronic Heart Failure

DWORF DWARF open reading frame

EC50 Half maximal effective concentration

HO-1 Heme oxygenase 1

Keap-1 Kelch-like ECH-associated protein 1

LC3 Microtubule-associated protein 1A/1B-light chain 3

MPTP Mitochondrial permeability transition pore

NRF2 Nuclear factor erythroid 2-related factor 2

P62 Sequestosome 1

PLN Phospholamban

ROS Reactive oxygen species

SERCA2a Sarcoplasmic reticulum Ca²⁺-ATPase

mi/R Myocardial ischemia–reperfusion

mtROS Mitochondrial ROS

Declarations

Acknowledgments

This study was supported by grants from Mutua Madrileña (XIV Convocatoria de Ayudas a la Investigación en Salud, 2022 [AP180592022]). Dr. Lax is a Ramon and Cajal fellow in the Medicine Department, University of Murcia (RYC2019-027635-I) and is supported by MCIN/AEI/10.13039/501100011033 and the European Social Fund. Dr. Asensio-Lopez MC is a Torres Quevedo Researcher (PTQ2022-012539), Biocardio SL.

Author Contributions

M.d.C.A.-L. and A.L. conceived the study, generated the experimental data, and wrote and edited the manuscript. A.L. is the guarantor of this work and, as such, has full access to all the data in the study and takes responsibility for the integrity of the data and the accuracy of the analysis. Echocardiography procedures, measurements, and interpretation were carried out by M.J.F.d.P., M.R.B., and S.P.-O., who helped with the analysis data. YS contributed to writing the discussion. D.P.-F., F.S., and J.J.F. helped with the analysis, contributed to writing the discussion, and edited the manuscript.

Competing Interests

The authors declare no competing interests.

Footnotes

Publisher's note Springer Nature remains neutral with regard to jurisdictional claims in published maps and institutional affiliations.

These authors contributed equally: Asensio-Lopez MC, Ruiz-Ballester M.

Supplementary information

Supplementary information accompanies the manuscript on the Experimental & Molecular Medicine website (<http://www.nature.com/emml/>)

References

1. Tsao, C. W. *et al.* Heart Disease and Stroke Statistics-2022 Update: A Report From the American Heart Association. *Circulation* **145**, E153–E639 (2022).
2. Miura, T. & Miki, T. Limitation of myocardial infarct size in the clinical setting: current status and challenges in translating animal experiments into clinical therapy. *Basic Res. Cardiol.* **103**, 501–513 (2008).
3. Eltzschig, H. K. & Eckle, T. Ischemia and reperfusion—from mechanism to translation. *Nat. Med.* **17**, 1391–1401 (2011).
4. Liang, S., Ping, Z. & Ge, J. Coenzyme Q10 Regulates Antioxidative Stress and Autophagy in Acute Myocardial Ischemia-Reperfusion Injury. *Oxid. Med. Cell. Longev.* **2017**, (2017).
5. Aldakkak, M., Camara, A. K. S., Heisner, J. S., Yang, M. & Stowe, D. F. Ranolazine reduces Ca²⁺ overload and oxidative stress and improves mitochondrial integrity to protect against ischemia reperfusion injury in isolated hearts. *Pharmacol. Res.* **64**, 381–392 (2011).
6. Roger, V. L. *et al.* Executive summary: heart disease and stroke statistics—2012 update: a report from the American Heart Association. *Circulation* **125**, 188–197 (2012).
7. Krum, H. & Teerlink, J. R. Medical therapy for chronic heart failure. *Lancet (London, England)* **378**, 713–721 (2011).
8. Gutierrez, J., Ballinger, S. W., Darley-Usmar, V. M. & Landar, A. Free radicals, mitochondria, and oxidized lipids: the emerging role in signal transduction in vascular cells. *Circ. Res.* **99**, 924–932 (2006).
9. Takimoto, E. & Kass, D. A. Role of oxidative stress in cardiac hypertrophy and remodeling. *Hypertens. (Dallas, Tex. 1979)* **49**, 241–248 (2007).
10. Santos, C. X. C., Anilkumar, N., Zhang, M., Brewer, A. C. & Shah, A. M. Redox signaling in cardiac myocytes. *Free Radic. Biol. Med.* **50**, 777–793 (2011).
11. Shen, Y., Liu, X., Shi, J. & Wu, X. Involvement of Nrf2 in myocardial ischemia and reperfusion injury. *Int. J. Biol. Macromol.* **125**, 496–502 (2019).
12. Chen, Q. M. & Maltagliati, A. J. Nrf2 at the heart of oxidative stress and cardiac protection. *Physiol. Genomics* **50**, 77–97 (2018).

13. Chen, Q. M. Nrf2 for protection against oxidant generation and mitochondrial damage in cardiac injury. *Free Radic. Biol. Med.* **179**, 133–143 (2022).
14. Wang, Z., Zhang, Y., Wang, L., Yang, C. & Yang, H. NBP Relieves Cardiac Injury and Reduce Oxidative Stress and Cell Apoptosis in Heart Failure Mice by Activating Nrf2/HO-1/Ca²⁺-SERCA2a Axis. *Evid. Based. Complement. Alternat. Med.* **2022**, (2022).
15. Weber, D. K. *et al.* Structural basis for allosteric control of the SERCA-Phospholamban membrane complex by Ca²⁺ and phosphorylation. *Elife* **10**, (2021).
16. Li, A. *et al.* The transmembrane peptide DWORF activates SERCA2a via dual mechanisms. *J. Biol. Chem.* **296**, (2021).
17. Fisher, M. E. *et al.* Dwarf open reading frame (DWORF) is a direct activator of the sarcoplasmic reticulum calcium pump SERCA. *Elife* **10**, (2021).
18. Sitsel, A. *et al.* Structures of the heart specific SERCA2a Ca²⁺-ATPase. *EMBO J.* **38**, e100020 (2019).
19. D’Oria, R. *et al.* The Role of Oxidative Stress in Cardiac Disease: From Physiological Response to Injury Factor. *Oxid. Med. Cell. Longev.* **2020**, (2020).
20. Brown, R. B. Phosphate toxicity and SERCA2a dysfunction in sudden cardiac arrest. *FASEB J.* **37**, e23030 (2023).
21. Cui, W. *et al.* AEOL 10150 alleviates radiation-induced innate immune responses in nonhuman primate lung tissue. *Health Phys.* **121**, 331 (2021).
22. Kliment, C. R. *et al.* Extracellular superoxide dismutase regulates cardiac function and fibrosis. *J. Mol. Cell. Cardiol.* **47**, 730–742 (2009).
23. Zhang, X. R., Zhou, W. X. & Zhang, Y. X. Improvements in SOD mimic AEOL-10150, a potent broad-spectrum antioxidant. *Mil. Med. Res.* **5**, (2018).
24. Garofalo, M. C. *et al.* A pilot study in rhesus macaques to assess the treatment efficacy of a small molecular weight catalytic metalloporphyrin antioxidant (AEOL 10150) in mitigating radiation-induced lung damage. *Health Phys.* **106**, 73–83 (2014).
25. Sebastião, M. J. *et al.* Human cardiac progenitor cell activation and regeneration mechanisms: exploring a novel myocardial ischemia/reperfusion in vitro model. *Stem Cell Res. Ther.* **10**, (2019).
26. Murigi, F. N. *et al.* Dose Optimization Study of AEOL 10150 as a Mitigator of Radiation-Induced Lung Injury in CBA/J Mice. *Radiat. Res.* **184**, 422–432 (2015).
27. Salin, K. *et al.* Using the MitoB method to assess levels of reactive oxygen species in ecological studies of oxidative stress. *Sci. Rep.* **7**, (2017).
28. Smith, P. K. *et al.* Measurement of protein using bicinchoninic acid. *Anal. Biochem.* **150**, 76–85 (1985).
29. Zacchigna, S. *et al.* Towards standardization of echocardiography for the evaluation of left ventricular function in adult rodents: a position paper of the ESC Working Group on Myocardial Function. *Cardiovasc. Res.* **117**, 43–59 (2021).
30. Soler, F. *et al.* PDE2 activity differs in right and left rat ventricular myocardium and differentially regulates β 2 adrenoceptor-mediated effects. *Exp. Biol. Med.* **240**, 1205 (2015).

31. Schaaf, T. M. *et al.* Live-Cell Cardiac-Specific High-Throughput Screening Platform for Drug-Like Molecules That Enhance Ca²⁺ Transport. *Cells* 2020, Vol. 9, Page 1170 **9**, 1170 (2020).
32. Lytton, J., Westlin, M. & Hanley, M. R. Thapsigargin inhibits the sarcoplasmic or endoplasmic reticulum Ca-ATPase family of calcium pumps. *J. Biol. Chem.* **266**, 17067–17071 (1991).
33. Asensio-Lopez, M. C. *et al.* The miRNA199a/SIRT1/P300/Yy1/sST2 signaling axis regulates adverse cardiac remodeling following MI. *Sci. Rep.* **11**, (2021).
34. Tabata Fukushima, C. *et al.* Reactive oxygen species generation by reverse electron transfer at mitochondrial complex I under simulated early reperfusion conditions. *Redox Biol.* **70**, (2024).
35. Niccoli, G., Burzotta, F., Galiuto, L. & Crea, F. Myocardial No-Reflow in Humans. *J. Am. Coll. Cardiol.* **54**, 281–292 (2009).
36. Kasai, S., Shimizu, S., Tatara, Y., Mimura, J. & Itoh, K. Regulation of Nrf2 by Mitochondrial Reactive Oxygen Species in Physiology and Pathology. *Biomol.* 2020, Vol. 10, Page 320 **10**, 320 (2020).
37. Wu, X., Wei, J., Yi, Y., Gong, Q. & Gao, J. Activation of Nrf2 signaling: A key molecular mechanism of protection against cardiovascular diseases by natural products. *Front. Pharmacol.* **13**, (2022).
38. Zhu, Z., Li, J. & Zhang, X. Astragaloside IV Protects Against Oxidized Low-Density Lipoprotein (ox-LDL)-Induced Endothelial Cell Injury by Reducing Oxidative Stress and Inflammation. *Med. Sci. Monit.* **25**, 2132–2140 (2019).
39. Orellana-Urzúa, S., Briones-Valdivieso, C., Chichiarelli, S., Saso, L. & Rodrigo, R. Potential Role of Natural Antioxidants in Countering Reperfusion Injury in Acute Myocardial Infarction and Ischemic Stroke. *Antioxidants* 2023, Vol. 12, Page 1760 **12**, 1760 (2023).
40. Garofalo, M. *et al.* The delayed pulmonary syndrome following acute high-dose irradiation: a rhesus macaque model. *Health Phys.* **106**, 56–72 (2014).
41. Macvittie, T. J. *et al.* AEOL 10150 Mitigates Radiation-Induced Lung Injury in the Nonhuman Primate: Morbidity and Mortality are Administration Schedule-Dependent. *Radiat. Res.* **187**, 298–318 (2017).
42. Bowler, R. P. *et al.* A catalytic antioxidant (AEOL 10150) attenuates expression of inflammatory genes in stroke. *Free Radic. Biol. Med.* **33**, 1141–1152 (2002).
43. Mbikou, P., Rademaker, M. T., Charles, C. J., Richards, M. A. & Pemberton, C. J. Cardiovascular effects of DWORF (dwarf open reading frame) peptide in normal and ischaemia/reperfused isolated rat hearts. *Peptides* **124**, (2020).
44. Makarewich, C. A. *et al.* The DWORF micropeptide enhances contractility and prevents heart failure in a mouse model of dilated cardiomyopathy. *Elife* **7**, (2018).

Figures

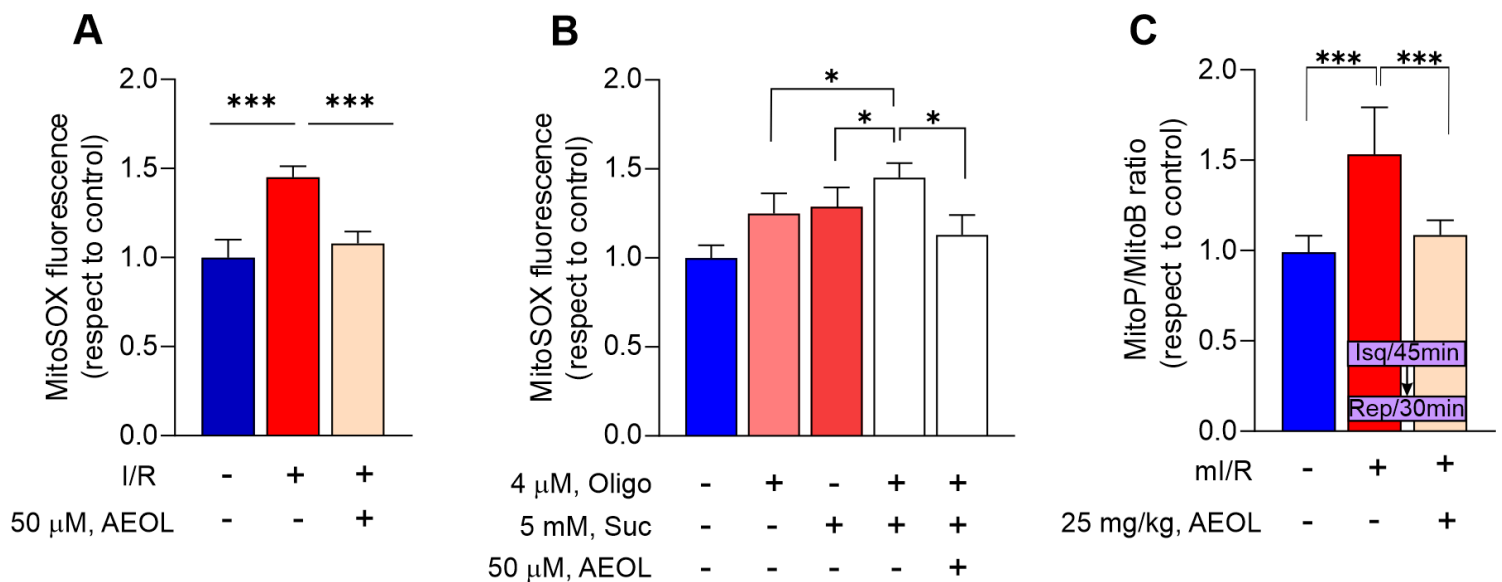


Figure 1

AEOL-10150 reduces ROS production upon reoxygenation/reperfusion. (A) ROS production assessed with the mitochondrial superoxide indicator MitoSOX Red in hiPSCMs subjected to simulated ischemia (1% O₂, no glucose) for 45 min followed by 24 h reoxygenation (I/R model). Cells were treated with AEOL (50 μ M) or vehicle (saline solution; 0.9% NaCl) at the onset of reoxygenation. (B) ROS production in hiPSCMs treated with dimethyl succinate (Suc) and oligomycin (Oligo) for 2 h. (C) Inhibitory effect of AEOL on ROS generation assessed 30 min after ml/R. Mice undergoing the ml/R procedure were treated with a subcutaneous injection of AEOL (25 mg/kg) or vehicle (DPBS) 15 min after reperfusion onset, and ROS were measured from the oxidation of MitoB injected 4 h before the procedure. Data are from n=5 independent assays per group for *in vitro* procedures and n=7 mice per group for *in vivo* procedures. Quantitative data are presented as mean \pm standard error of the mean (SEM). ***p < 0.001; *p < 0.05, determined by one-way ANOVA followed by post hoc Bonferroni correction. BS, blood samples; CS, cardiac samples; I/R, ischemia-reperfusion; Oligo, oligomycin; Suc, succinate; wks, weeks. Other abbreviations are defined in the abbreviations list.

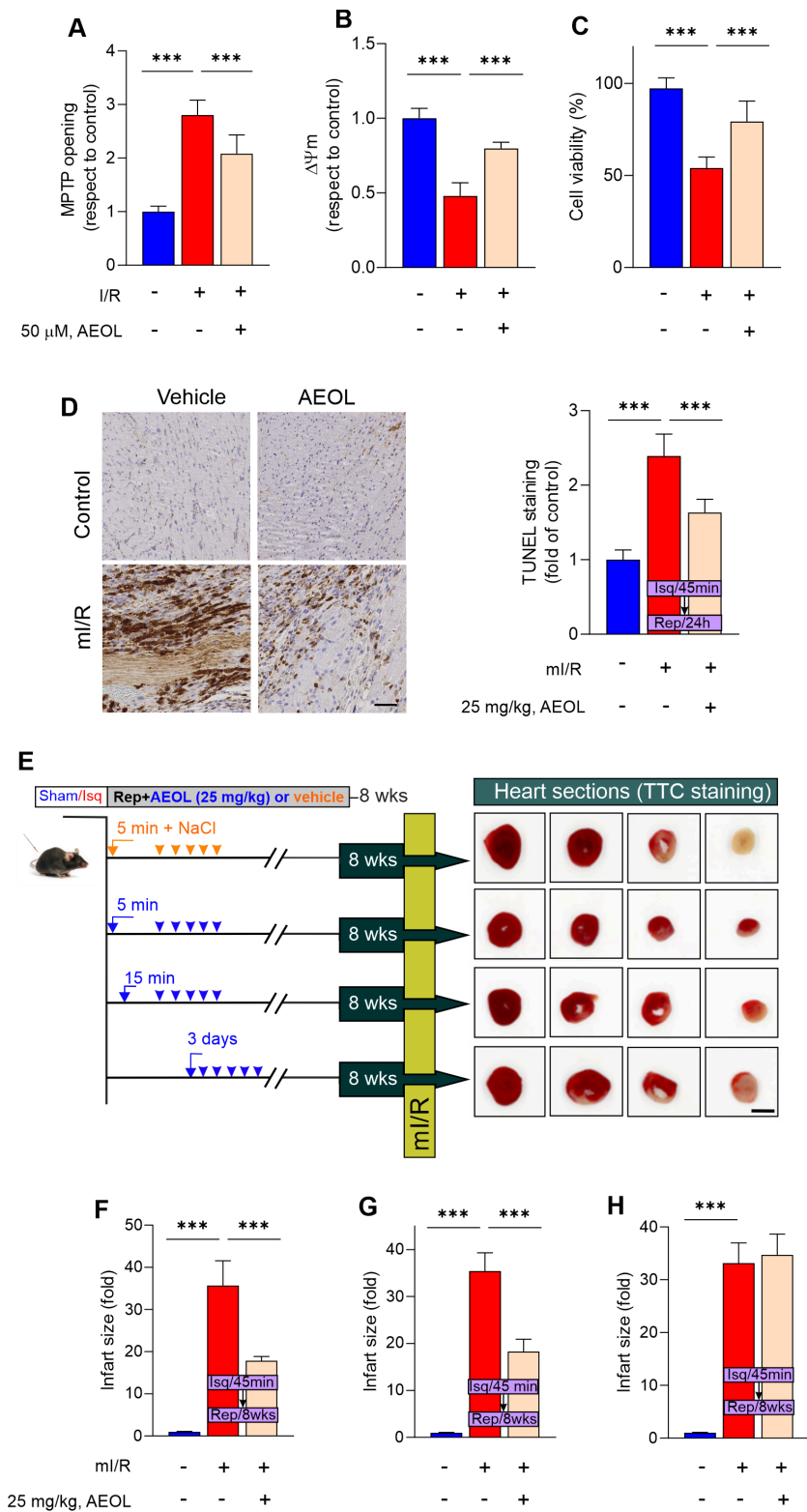


Figure 2

AEOL treatment reduces in the reactive oxygen species (ROS) surge triggered by reperfusion and protects against acute ischemia–reperfusion (I/R) injury. (A–C), hiPSCMs subjected to ischemia (1% O₂) for 45 min followed by 24 h reoxygenation (I/R model) were treated with AEOL (50 μ M) and assayed for (A) mitochondrial permeability transition pore opening, (B) mitochondrial potential ($\Delta\psi_m$), and (C) cell viability. (D), Representative images and quantification of TUNEL staining in LV sections from mice subjected to

ml/R and recovered for 24 h. Mice were treated as indicated with 25 mg/kg AEOL or vehicle (0.9% NaCl) 15 min after starting reperfusion. Scale bar, 50 μ m. (E) Experimental design for determination of myocardial infarct size in mice subjected to ml/R and recovered for 8 weeks, with serial daily treatment with AEOL or vehicle (0.9% NaCl) starting 5 min, 15 min, or 3 days after reperfusion onset. Representative photographs show TTC staining 8 weeks post-reperfusion. (F-H) Effect of AEOL administration 5 min (F), 15 min (G), or 3 days (H) after reperfusion onset on infarct size determined at 8-weeks post-ml/R. Quantifications were obtained from n=5 independent assays per group for *in vitro* procedures and n=7 mice per group for *in vivo* assays. Quantitative data are presented as mean \pm SEM. ***p < 0.001 determined by one-way ANOVA followed by post hoc Bonferroni correction. TTC, 2,3,5-triphenyltetrazolium chloride. Other abbreviations are defined in the abbreviations list.

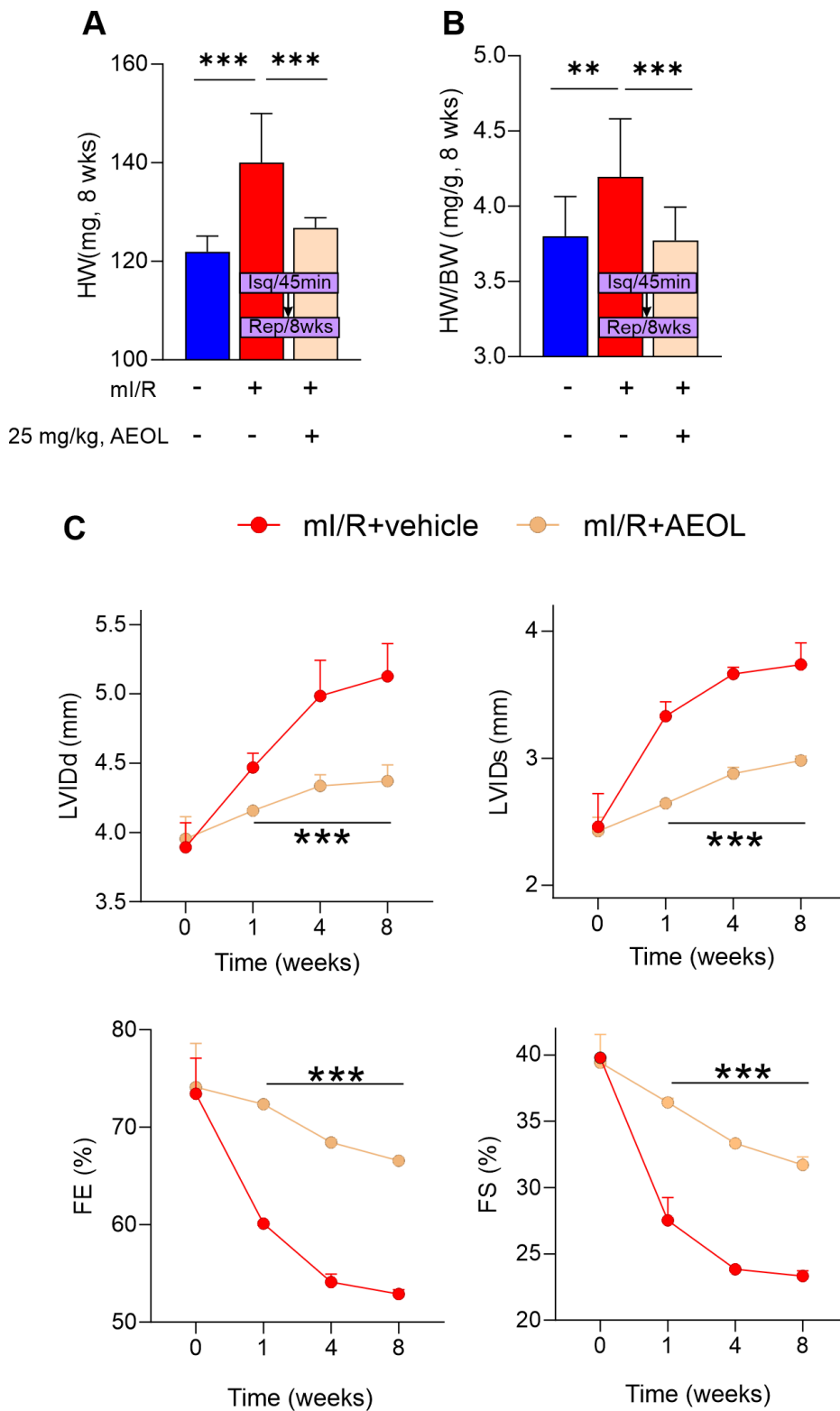


Figure 3

AEOL treatment in acute-phase ml/R injury improves cardiac function. (A, B) Heart weight (HW) and HW/body-weight (BW) ratio in mice subjected to ml/R, treated with AEOL or vehicle (0.9% NaCl) 15 min after reperfusion onset, and recovered for 8 weeks. (C) Evolution of echocardiography measures of cardiac function. Functional benefits of short-term AEOL treatment vs vehicle after ml/R include smaller LV internal diameters at end diastole (LVIDd) and end systole (LVIDs) and better preserved % ejection fraction (% EF)

and % fractional shortening (% FS) (full echocardiography data are presented in Table 3). Data were obtained from n=7 mice/group, and are presented as mean ± SEM. ***p < 0.001; **p<0.01 determined by one-way ANOVA followed by post hoc Bonferroni correction. BW, body weight; HW, heart weight. Other abbreviations are defined in the abbreviations list.

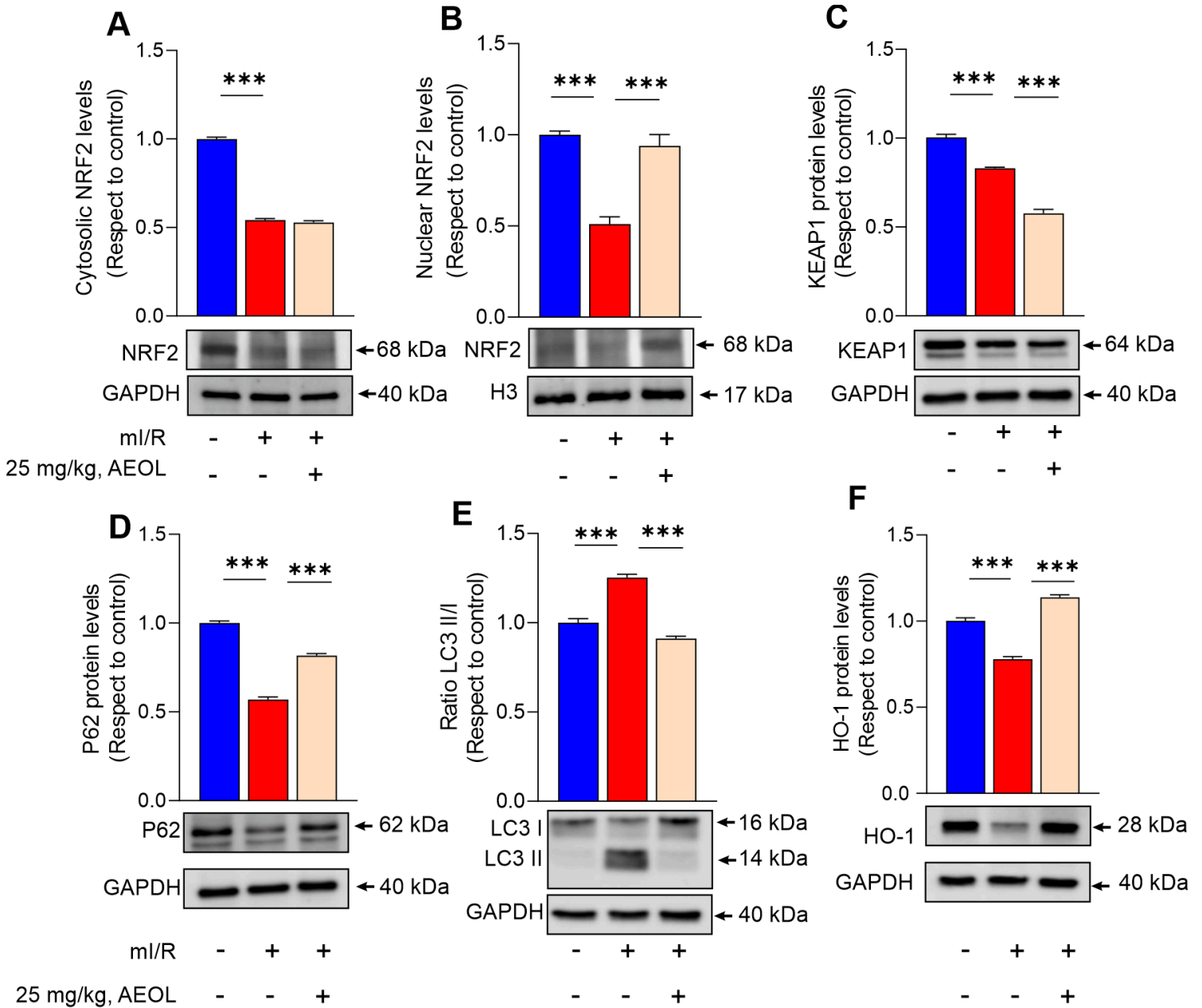


Figure 4

AEOL increases nuclear translocation of NRF2 and the transcriptional induction of downstream ARE-regulated genes in the infarct border zone. Mice subjected to mi/R were treated with AEOL or vehicle (0.9% NaCl) 15 min after reperfusion onset and sacrificed at 24 h post-mi/R. (A,B) Cytosolic and nuclear expression of NRF2 in the infarct border zone. (C) KEAP1 protein expression. (D) p62 protein expression levels. (E) LC3 II/LC3 I ratio. (F) HO-1 protein expression. Data are from n=7 mice/group and are presented as mean ± SEM. ***p < 0.001; determined by one-way ANOVA followed by post hoc Bonferroni correction. GAPDH, glyceraldehyde phosphate dehydrogenase; H3, histone H3; HO-1, heme oxygenase 1; KEAP1, kelch-

like ECH-associated protein 1; LC3, microtubule-associated protein 1A/1B-light chain 3; NRF2, nuclear factor erythroid 2-related factor 2; p62, sequestosome 1. Other abbreviations are defined in the abbreviations list.

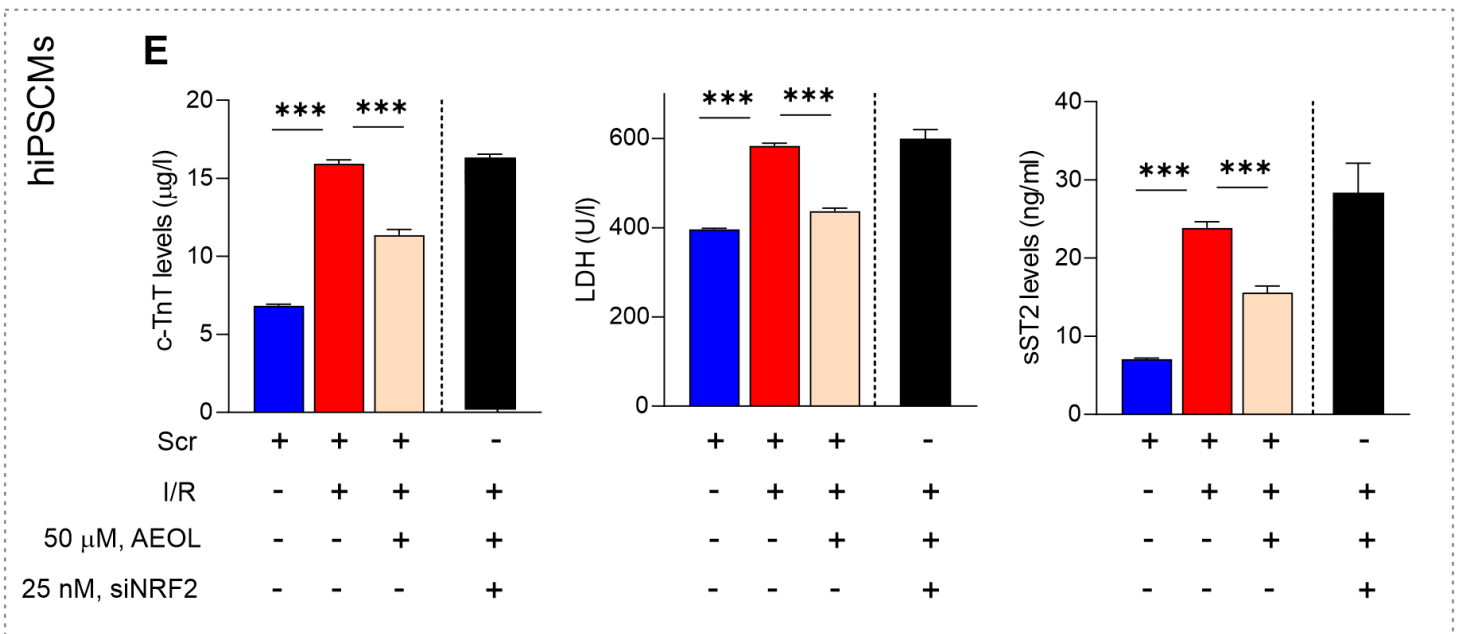
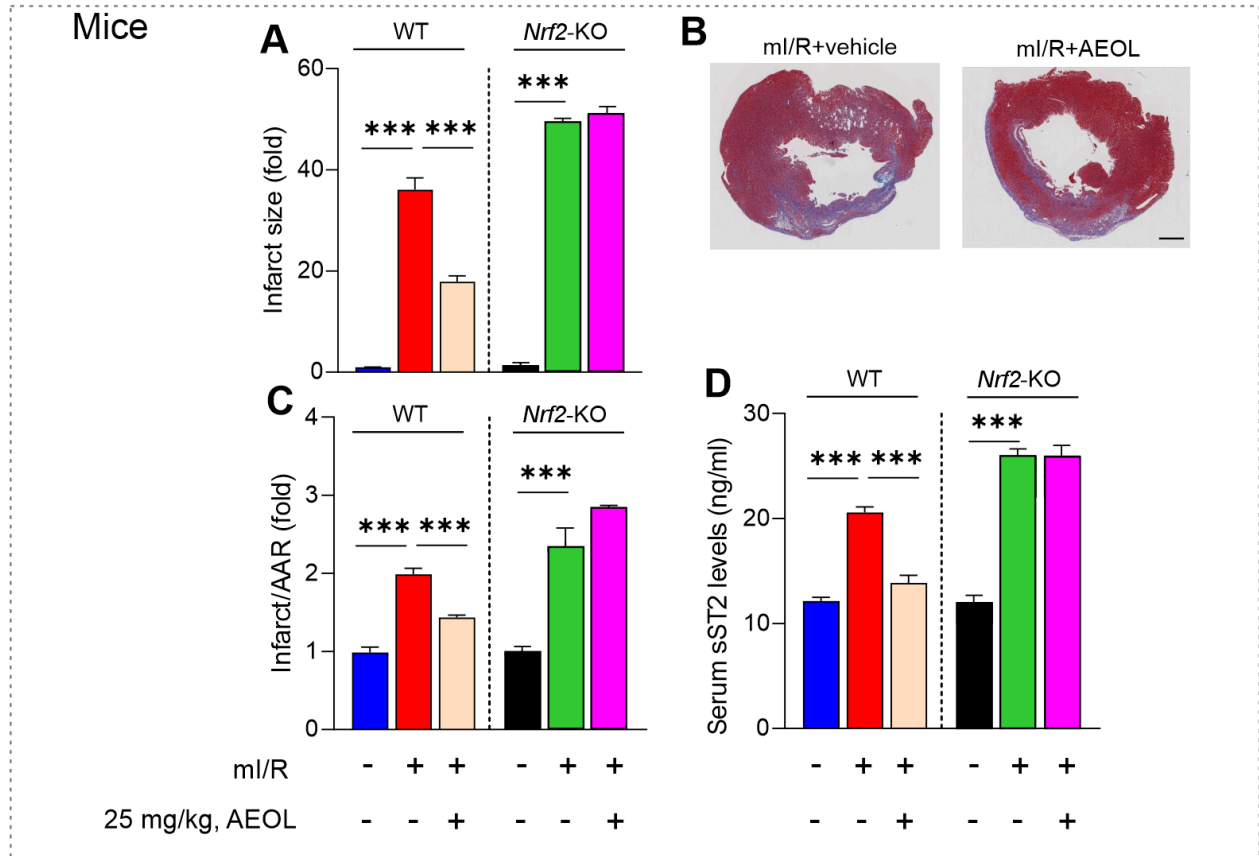


Figure 5

AEOL treatment ameliorates ml/R injury through NRF2. (A-D) Wild type and *Nrf2*-KO mice subjected to ml/R were treated with AEOL or vehicle (0.9% NaCl) 15 min after reperfusion onset and sacrificed at 8 weeks post-mi/R. (A) Infarct size calculated as the percentage of LV volume and expressed as fold of control. (B)

Representative LV sections from wild type mice obtained 8 weeks post-mI/R. Collagen in the scar is blue and myocytes are red. Scale bar, 0.5 cm. (C) Area-at-risk (AAR) calculated as the percentage of LV volume and expressed as fold of control. (D) Plasma sST2 in mice at 24 h post-mI/R. (E) hiPSCM culture supernatant content of c-TnT, LDH, and sST2 at 24 h after simulated I/R. Quantifications were obtained from n=7 mice per group for *in vivo* assays and n=5 independent assays per group for *in vitro* procedures. Quantitative data are presented as mean \pm SEM. ***p < 0.001 determined by one-way ANOVA followed by post hoc Bonferroni correction. AAR, area-at-risk; Scr, scramble; KO, knockout. Other abbreviations are defined in the abbreviations list.

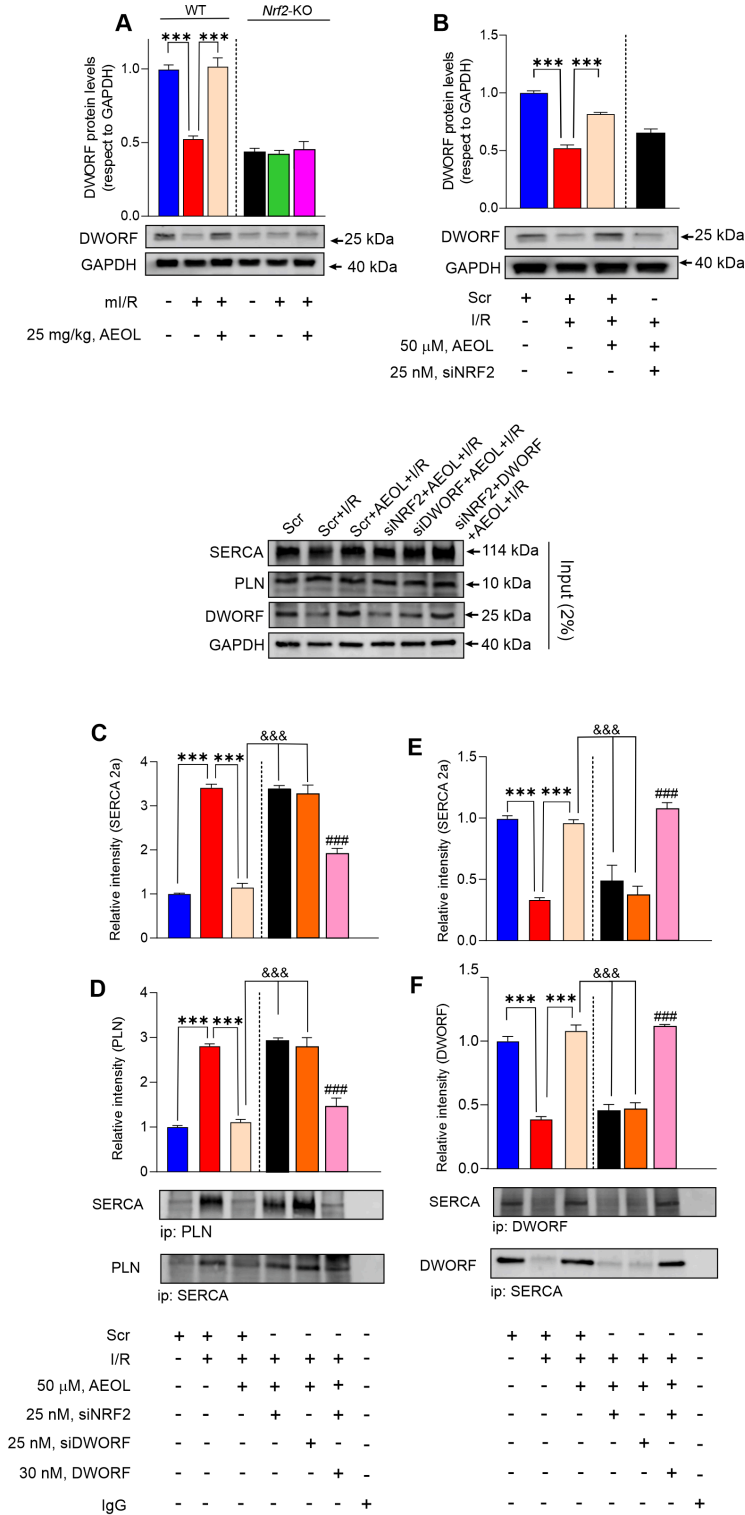


Figure 6

AEOL-induced DWORF upregulation displaces PLN from SERCA2a. (A) DWORF accumulation in the infarct border zone of mice 24 h after mI/R. Mice were treated with AEOL or vehicle (0.9% NaCl) 15 min after reperfusion onset. (B) DWORF accumulation in extracts of hiPSCMs subjected to the simulated I/R protocol (45 minutes ischemia followed by reoxygenation and maintenance for 24 h). Cells were transfected 48 h before simulated I/R with scrambled (Scr) or siNRF2 siRNA, as indicated, and treated with AEOL or vehicle (0.9% NaCl) at the onset of reoxygenation. (C-F) Co-immunoprecipitation analysis in hiPSCMs transfected as indicated with Scr, siNRF2, or siDWORF siRNA before simulated I/R. Cells were treated at the onset of reoxygenation with AEOL and DWORF, as indicated, and analyzed at 24 h after simulated I/R. (C, D) Co-immunoprecipitation and densitometry analysis of co-immunoprecipitated SERCA2a and PLN proteins. (E, F) Co-immunoprecipitation and densitometry analysis of co-immunoprecipitated SERCA2a and DWORF proteins. A representative input immunoblot is shown above panels C-F. Data were obtained from a sample size of n=7 mice per group for *in vivo* assays and n=5 independent assays per group for *in vitro* procedures and are presented as mean \pm SEM. ***p < 0.001; ### p<0.001 vs siNRF2+AEOL+I/R, determined by one-way ANOVA followed by post hoc Bonferroni correction. Abbreviations are defined in the abbreviations list.

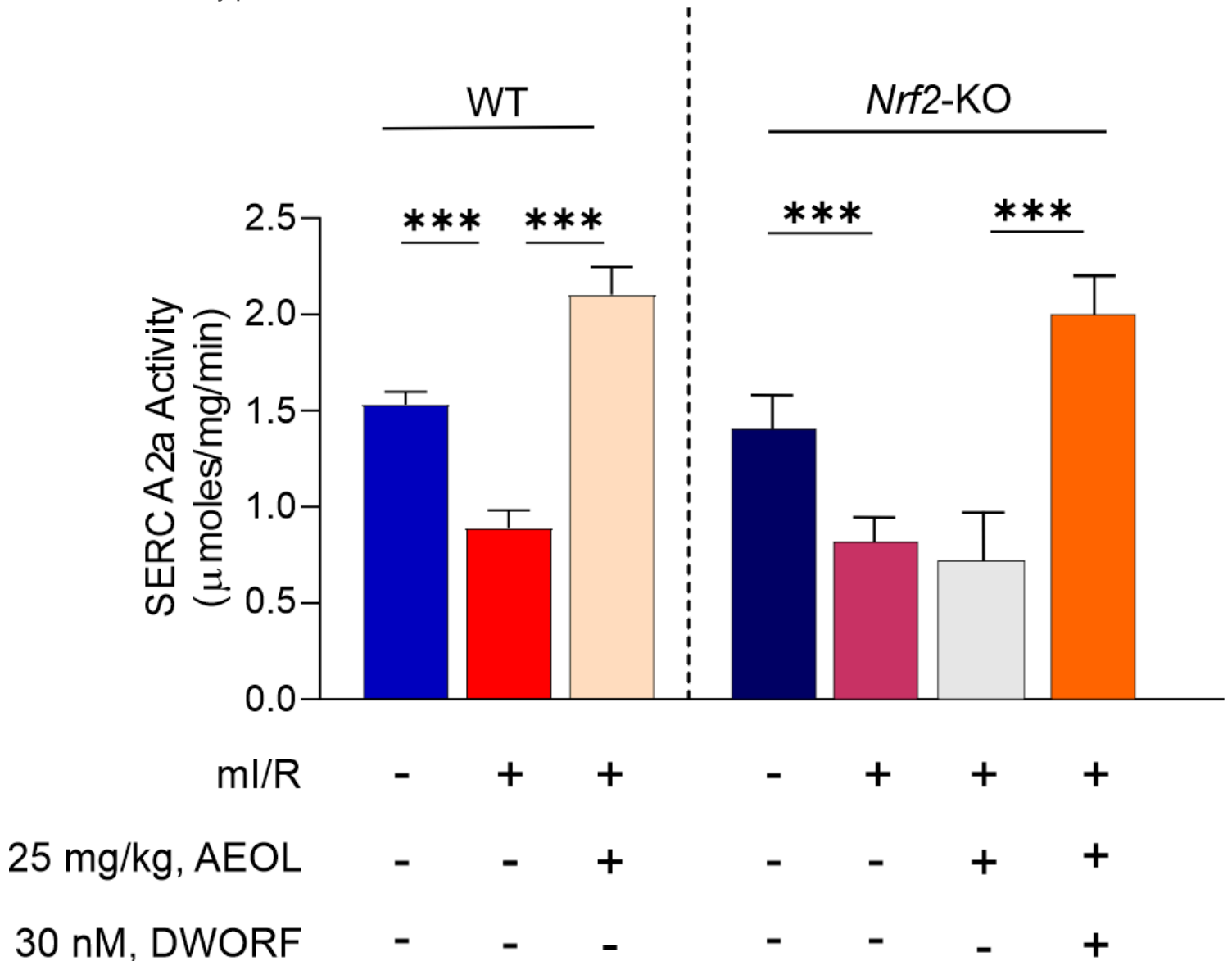


Figure 7

AEOL treatment enhances SERCA2a activity by upregulating DWORF expression. Maximal SERCA2a activity in the infarct border zone of wild type and *Nrf2*-KO mice subjected to ml/R, treated as indicated with AEOL and DWORF 15 min after reperfusion onset, and sacrificed at 24 h post-ml/R. Data were obtained from n=7 mice/group and are presented as mean values \pm SEM. ***p < 0.001, determined by one-way ANOVA followed by post hoc Bonferroni correction. Abbreviations are defined in the abbreviations list.

Supplementary Files

This is a list of supplementary files associated with this preprint. Click to download.

- [Supplementarydata.docx](#)
- [GraphicalAbstract.tif](#)